https://doi.org/10.5194/egusphere-2026-2
Preprint. Discussion started: 21 January 2026

Trait-based mechanisms underpin regional hotspot of diatom-driven carbon export in an oligotrophic gyre

Feng Li[1#], Hongzhen Jiang[1#], Linwei Liu[1], Zhouyi Jiang[1], Lu Huang[1], Kehui Feng[1], Zuozhu Wen[2], Xin Liu[2], Changping Chen[1], Kuanbo Zhou[2*], Junrong Liang[1*]

[1]School of Life Sciences, Key Laboratory of Ministry of Education for Coastal and Wetland Ecosystems, Xiamen Key Laboratory of Plant Genetics, Xiamen University, Xiamen 361102, Fujian, China.

[2]College of Ocean and Earth Sciences, State Key Laboratory of Marine Environment Science, Xiamen University, Xiamen 361102, Fujian, China.

#These authors contributed equally to this work.

*Corresponding author: sunljr@xmu.edu.cn (Junrong Liang); kbzhou@xmu.edu.cn (Kuanbo Zhou)

https://doi.org/10.5194/egusphere-2026-2
Preprint. Discussion started: 21 January 2026

Abstract

The oligotrophic subtropical gyres, vast yet nutrient-poor, pose challenges to our understanding of efficient carbon sequestration. Here, we integrate taxonomic, sediment trap, and metagenomic analyses to investigate the mechanisms underlying regionally heterogeneous and efficient diatom - mediated carbon export in the western North Pacific Subtropical Gyre. We discovered that within a vertically stratified nutrient regime, diatom communities displayed clear niche partitioning: *Navicula* and *Rhizosolenia* were enriched in the nutrient-depleted surface mixed layer, while *Nitzschia*, *Chaetoceros*, and *Thalassiosira* tended to dominate the deep chlorophyll maximum—reflecting hydrographic control over community assembly. This trait-based community structuring directly influenced the composition and magnitude of diatom carbon export, with fluxes ranging from 10^3 to 10^5 cells m^{-2} d^{-1} and an estimated 0.13–194.85 μg C m^{-2} d^{-1}. Total carbon export and export efficiency (carbon exported relative to production) was markedly enhanced at station affected by the Kuroshio (K2b), which was mainly driven by the large, carbon-rich *Rhizosolenia*, delineating a distinct regional hotspot. Critically, metagenomic analysis revealed a limited presence of bacteria genes encoding key carbohydrate-active enzymes capable of degrading diatom-derived fucose-containing sulfated polysaccharides (FCSP), indicating a key biochemical mechanism that may reduce organic matter remineralization and enhance flux preservation. Our findings establish a multi-process framework wherein hydrodynamic regimes select for export-prone diatom communities with specific functional traits (e.g., size, carbon content), and the biochemical resistance of their organic byproducts may synergistically promote efficient carbon export. This study deciphers the interacting controls on carbon sequestration heterogeneity in the oligotrophic ocean, with crucial implications for predicting the biological pump's response to global change.

Key words: diatom carbon export, microbial degradation resistance, fucose-containing sulfated polysaccharides (FCSP), North Pacific Subtropical Gyre, spatial variation, vertical stratification

https://doi.org/10.5194/egusphere-2026-2
Preprint. Discussion started: 21 January 2026

1.1 Introduction

The Biological Carbon Pump (BCP) is a cornerstone of the ocean's capacity to sequester atmospheric carbon, responsible for the majority of the dissolved inorganic carbon (DIC) gradient from the surface to the deep sea (Simon et al., 2025). Its efficiency, however, is not a simple function of primary production but is governed by a complex interplay of physical, ecological, and biogeochemical processes that control the composition of phytoplankton communities, the aggregation and sinking of particles, and the microbial remineralization of organic matter during descent (Kwon et al., 2009; McDonnell et al., 2015; Guidi et al., 2016; Tréguer et al., 2018).

Among phytoplankton, diatoms are often pivotal to efficient carbon export (Tréguer et al., 2018; Zhang et al., 2018; Stukel et al., 2023). Their silica frustules provide ballast, enhancing particle sinking velocity (Tréguer et al., 2018). Perhaps more critically, many diatoms produce specific extracellular polymers, notably fucose-containing sulfated polysaccharides (FCSPs), which drive the formation of sticky, gel-like transparent exopolymer particles (TEP) (Vidal-Melgosa et al., 2021). These TEP facilitate particle aggregation and, due to their complex sulfated structure, exhibit significant resistance to bacterial degradation (Vidal-Melgosa et al., 2021). This combination of physical (ballasting) and biochemical (polymer-mediated aggregation and preservation) traits enables diatoms to contribute disproportionately more to deep carbon flux relative to their share of primary production (Henson et al., 2019). The ultimate fate of this diatom-derived carbon is further regulated by the metabolic capabilities of heterotrophic bacteria, whose suite of carbohydrate-active enzymes (CAZymes) determines the degradation rates of key polysaccharides like laminarin, mannans, and FCSPs. The balance between particle export and microbial degradation thus represents a fundamental biogeochemical control point for carbon sequestration.

A central paradox emerges in the vast oligotrophic ecosystems of the subtropical gyres, such as the North Pacific Subtropical Gyre (NPSG). Characterized by strong stratification, chronic nutrient limitation, and dominance by picophytoplankton, the NPSG is often considered a "marine desert" with a weak biological pump (Karl et al., 2012; Letscher et al., 2016; Xiu & Chai, 2020; Dai et al., 2023). Diatoms are typically sparse, raising a key mechanistic question: Can the coupled physical-biological processes that underpin diatom-mediated carbon export operate efficiently under such persistently oligotrophic conditions? While episodic diatom blooms in the eastern

https://doi.org/10.5194/egusphere-2026-2
Preprint. Discussion started: 21 January 2026

NPSG are known to drive substantial export (Scharek et al., 1999; Villareal et al., 2011; Karl et al., 2012), the functioning and efficiency of diatom communities during non-bloom periods—particularly in the understudied western NPSG—remain poorly constrained. Furthermore, the strongly stratified water column creates distinct niche environments: a nutrient-depleted surface layer (NDL) overlying a nutrient-replete deep layer (NRL) (Dore et al., 2008; Dai et al., 2023). This vertical physicochemical gradient likely promotes differentiation in diatom community structure, which may in turn lead to heterogeneity in the magnitude, composition, and efficiency of exported carbon.

This study employed an integrated approach to investigate the diatom-driven carbon export and its potential controls in the western NPSG. We combine taxonomic community analysis, sediment trap flux measurements, and metagenomic profiling of bacterial CAZymes across four biogeochemically distinct subregions. Our objectives are to: (1) describe the spatial and vertical structure of diatom communities and their carbon export fluxes; (2) assess regional heterogeneity in export efficiency (carbon exported relative to production); and (3) evaluate a potential biochemical mechanism—the limited bacterial degradation potential for diatom-derived FCSPs—that may enhance carbon export in this oligotrophic system. By linking community ecology, flux biogeochemistry, and microbial genomics, this work aims to provide a mechanistic framework for understanding how interacting processes can sustain carbon export efficiency even in nutrient-limited oceans.

2 Material and methods

2.1 Western NPSG and sampling stations

Sampling was carried out in the western NPSG during two research cruises on the R/V *Tan Kah Kee*: the KK2003 expedition in summer (July–August 2020) and the KK2007 expedition in winter (January–February 2021). A total of five stations were occupied, spanning four biogeochemical regions: K2b (125ºE, 20ºN) in the Kuroshio region, M35 (155ºE, 33ºN) in the Kuroshio Extension area, WPS (140ºE, 20ºN) and M22 (155ºE, 20ºN) within the NPSG interior, and K8a (155ºE, 12.5ºN) in the NEC area (Fig. 1a).

https://doi.org/10.5194/egusphere-2026-2
Preprint. Discussion started: 21 January 2026

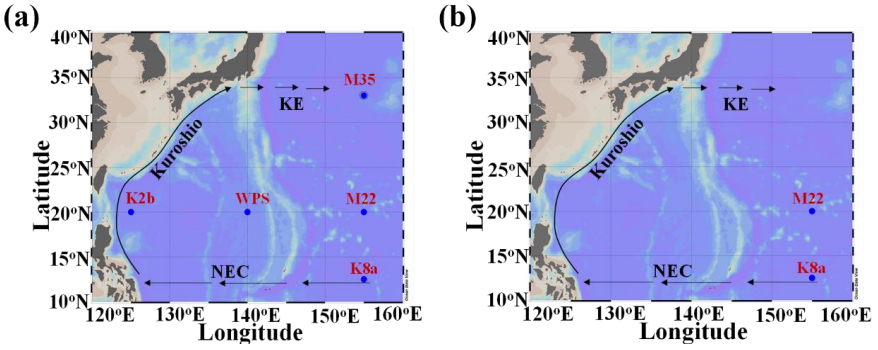

Fig. 1 Sampling stations in the western North Pacific Subtropical Gyre (NPSG) during summer (Chinese KK2003 cruise) and winter (Chinese KK2007 cruise). (a) Sampling stations established in summer, (b) Sampling stations established in winter.

2.2 Sample collections

Water samples for diatom taxonomy and abundance analysis were collected from three predefined depths: the surface mixed layer (5 m), the deep chlorophyll *a* maximum (DCM), and 200 m, using Niskin-X bottles. During the summer cruise, all five stations were sampled (Fig. 1A), with the DCM depth varying station-specifically: K2b (110 m), WPS (145 m), M22 (155 m), K8a (150 m), and M35 (95 m). Winter sampling was conducted only at stations M22 and K8a due to rough sea conditions (Fig. 1b).

Settling particulate matter for diatom export flux was collected with custom-made sediment traps deployed at 50 m, 100 m, and 200 m. Traps were successfully retrieved only at stations K2b, M22, and K8a in the summer cruise, enabling quantification of diatom carbon export fluxes at these sites.

For metagenomic analysis, a total of 39 samples were obtained: during summer, seawater from 5 m and the DCM at all five stations was filtered in situ (100–120 L per sample) through 0.2 μm (142 mm) polycarbonate membranes using a high-volume pump; each filter was subdivided into eight aliquots, stored in cryovials, and kept at –80°C. In winter, water sampling was additionally performed at 200 m depth at station M22.

A complete summary of sampling stations and depths is provided in Table S1.

2.3 Environmental data

https://doi.org/10.5194/egusphere-2026-2
Preprint. Discussion started: 21 January 2026

The environmental data during sampling were measured by the team led by Du (Du et al., 2024).

2.4 Diatom taxonomy and counting

For diatom taxonomic analysis, 20 L of seawater was collected at each sampling site and immediately fixed with Lugol's solution (1.5% vol/vol). Samples were stored in opaque plastic bags to avoid light exposure prior to laboratory processing. Given the typical low diatom abundance in oligotrophic waters and the prevalence of small-sized taxa, a concentration-based approach combined with filtration was selected to improve detection sensitivity (Jiang et al., 2019) as conventional filtration methods may fail to capture smaller cells due to pore size constraints (Zhang et al., 2022).

For the detailed, samples underwent sequential sedimentation in the laboratory. Following three days of settling, two-thirds of the supernatant was carefully removed via siphoning. The removed supernatant was filtered through an 8-μm nylon mesh to prevent the loss of floating species, while the remaining sample was gently resuspended and transferred to a new container for further concentration. This procedure was repeated until a final volume of 10 mL was obtained. Throughout processing, meticulous care was taken to minimize cell damage, including gentle shaking and slow liquid transfers, to preserve fragile, lightly silicified frustules. Although the method may slightly underestimate larger or more fragile taxa (e.g., *Rhizosolenia*), it effectively retained intact cells of small species such as *Nitzschia*, *Navicula*, *Eunotogramma*, and *Protoraphis*, enabling reliable inter-station comparison of diatom community composition.

For the identification and counting of diatom species, 100 μL of the resulting concentrate was transferred to a 0.1-mL phytoplankton counting chamber and analyzed using a light microscope (Olympus BX51) at 200× and 400× magnifications (Jiang et al., 2019). Diatom identification was conducted with the support of standard taxonomic references. Triplicate counting was carried out to determine the abundance of diatom species.

Diatom abundance (N, cells L^{-1}) was calculated using the following formulas:

$$N=（N_1 \times V_2）/（V_1 \times V） \quad (1)$$

https://doi.org/10.5194/egusphere-2026-2
Preprint. Discussion started: 21 January 2026

In equation 1, N represents the abundance of diatoms (cells L^{-1}). N_1 denotes the count of diatoms in a specific volume of concentrated sample (cells). V_2 indicates the total post-concentration sample volume (mL). V_1 refers to the volume used for observation (μL), and V represents the pre-concentration total sample volume (L).

2.5 Estimation of carbon biomass

The estimation of total phytoplankton carbon biomass was obtained by converting chlorophyll *a* (Chl *a*) concentration into carbon equivalents using the carbon-to- Chl *a* ratio (C: Chl *a*), with C: Chl *a* value derived from in situ measurements at the ALOHA station at corresponding depths (Wang et al., 2015; Liu et al., 2016). Total Chl *a* was quantified by HPLC analysis: filters were extracted with 2 ml of N, N-dimethylformamide, and the extracts were analyzed using an Agilent 1100 series HPLC system (Huang et al., 2010).

For the estimation of diatom carbon biomass, the average carbon content among known species within each genus was adopted as the representative carbon content for that genus. Most species-specific carbon content values were compiled from existing literature (Harrison et al., 2015; Chitari & Anil, 2017; Chen et al., 2023; Rath & Mitbavkar, 2023). For genera lacking reported carbon content data, carbon content was estimated through established proxy methods. In cases where only cellular volume data were available, carbon content was derived using the volume-to-carbon conversion relationship proposed by Menden-Deuer & Lessard (2000). For taxa with no available carbon or volume measurements, biovolume was calculated based on cell dimensions using appropriate geometric models (Sun & Liu, 2003), and carbon content was subsequently estimated using the empirical formula of Eppley et al. (1970). The resulting average carbon biomass values for each genus included in this study are summarized in Table S2.

2.6 Diatom community analysis

Differences in diatom community structure between sampling sites were investigated with a non-metric multidimensional scaling (NMDS) analysis of Bray–Curtis dissimilarity using the vegan (version 2.5–1) package (Oksanen et al., 2019) in R (version 3.4.1).

Diatom community diversity was assessed based on carbon biomass using three

https://doi.org/10.5194/egusphere-2026-2
Preprint. Discussion started: 21 January 2026

α diversity indices: Species richness index (Pielou, 1966), Simpson index (Siqueiros Beltrones et al., 2025), and Pielou evenness index (Pielou, 1966). Species richness simply counts the number of species present, providing a basic measure of biodiversity (Taurozzi & Scalici, 2025). The Simpson diversity index was calculated as 1 − D, which reflects the dominance structure within the community by emphasizing the probability that two randomly selected individuals belong to the same species (Buzas & Hayek, 2005). Pielou's evenness index (J) was applied to quantify the uniformity of species abundance distribution, standardizing the Shannon diversity value to a scale ranging from 0 to 1 (Kunakh et al., 2023).

2.7 Fluxes of diatom cells and the estimated carbon biomass

Floating sediment traps were deployed at selected sites for 72 hours. Each trap consisted of 12 tubes (10 cm diameter × 50 cm height) per depth. After collection, one tube was randomly selected for concentration, yielding a final volume of 20 mL. From this, 5 mL aliquots were analyzed using an inverted microscope and the Utermöhl method (Utermöhl, 1958) at 200× and 400× magnifications. Owing to the scarcity of samples, the results of three counts from a single tube will be regarded as the final value. The same principle applies to the subsequent particulate organic carbon (POC) flux and biogenic silica (BSi) flux.

Diatom cells flux (F) was calculated as:

$$F = (N_1 \times N_2) / (V_1 \times A \times T) \quad (2)$$

where F represents diatom cells flux (cells m^{-2} d^{-1}), N_1 is the observed diatom count in a specific sample volume (cells), V_2 is the post-concentration sample volume (mL), V_1 is the volume used for sample observation (μL), A denotes the collector's cross-sectional area (m^3), and T is the sediment trap's collection time (d).

The estimated carbon biomass flux for each site was acquired by converting the cell fluxes of all species at the site into the sum of the average carbon biomass values corresponding to the genus of each species.

2.8 The fluxes of total POC and BSi

Total POC concentration in the sediment traps was quantified using an elemental

https://doi.org/10.5194/egusphere-2026-2
Preprint. Discussion started: 21 January 2026

analyzer-isotope ratio mass spectrometer (EA-IRMS; vario PYRO cube coupled with Isoprime 100) following the removal of inorganic carbon via acid fumigation with concentrated HCl (24 h, room temperature) (Wang et al., 2025). A procedural carbon blank correction (<6 μg C) was applied to all POC measurements.

For BSi analysis, samples were oven-dried (50 °C, 24 h) and subjected to a one-step wet-alkaline digestion (0.2 M NaOH, 100 °C, 40 min) to solubilize particulate silica (Lam et al., 2018). The dissolved silicon concentrations were then determined spectrophotometrically by measuring the silico-molybdate blue complex using a Technicon AA3 Auto-Analyzer (Bran + Luebbe GmbH). Replicate analyses of selected filter samples confirmed a methodological uncertainty of <10% (Cao et al., 2020).

Sediment trap-derived POC export fluxes were calculated as follows:

$$F=[POC]/(A\times T) \quad (3)$$ (Belcher et al., 2023)

Where [POC] are the POC concentrations collected by the traps. A denotes the collector's cross-sectional area (m^3), and T is the sediment trap's collection time (d).

The same calculation was carried out for BSi.

$$F=[BSi]/(A\times T) \quad (4)$$ (Belcher et al., 2023)

2.9 Metagenomic analysis and MAG reconstruction

Total DNA was extracted following manufacturer protocols and sequenced on the Illumina HiSeq 2500 platform (PE 150) at Shanghai Majorbio Bio-pharm Technology Co., Ltd. Raw data were processed using Fastp (v0.20.0, https://github.com/OpenGene/fastp) to filter low-quality reads. Clean reads were assembled into contigs using MEGAHIT (v1.1.2), and open reading frames (ORFs) were predicted using MetaGene (Noguchi et al., 2006). Redundant genes were removed using CD-HIT (v4.6.1), resulting in a non-redundant gene catalog (Fu et al. 2012). Taxonomic and functional annotations were performed against the NR(http://ncbi.nlm.nih.gov/), EggNOG (http://eggnog.embl.de/), and KEGG (http://www.genome.jp/kegg) databases. Carbohydrate-active enzymes (CAZymes) were annotated using the dbCAN2 database(http://bcb.unl.edu/dbCAN2/download/Datab). Metagenome-assembled

https://doi.org/10.5194/egusphere-2026-2
Preprint. Discussion started: 21 January 2026

genomes (MAGs) were reconstructed using the ATLAS workflow (Kieser et al., 2020) with default parameters.

2.10 Data visualization and statistical analysis

Sampling map was visualized using Ocean Data View (ODV, v5.3.0). Both α-diversity indices and Spearman correlation analyses between diatom assemblages and physicochemical parameters were conducted using the R package *vegan* (Dixon, 2003). To evaluate significant differences in α-diversity indices, the Wilcoxon test was applied (Paul et al., 2016). Spearman's rank correlation analyses were calculated using Prism 9 (GraphPad Software) with two-tailed P-values and approximate 95% confidence intervals determined for all comparisons. (Schreiber et al., 2016). Comparative analyses of cell abundance and estimated carbon biomass across sampling sites or seasons were conducted using Student's t-test (Student, 1908), and data visualization (e.g. histograms) was performed using GraphPad Prism 9 (Li et al., 2024).

3. Results

3.1. Diatom abundance and community structure in water column

The western NPSG exhibited a distinct two-layer nutrient structure within the euphotic zone: a NDL and a NRL, as reflected in vertical profiles of temperature, salinity, nutrients, and Chl *a* (Fig. 2). Our sampling design targeted these layers, with the 5 m depth representing the NDL and DCM representing the NRL, across five stations spanning four biogeochemically distinct subregions (Kuroshio: K2b; Kuroshio Extension: M35; NPSG interior: M22, WPS; NEC: K8a).

https://doi.org/10.5194/egusphere-2026-2
Preprint. Discussion started: 21 January 2026

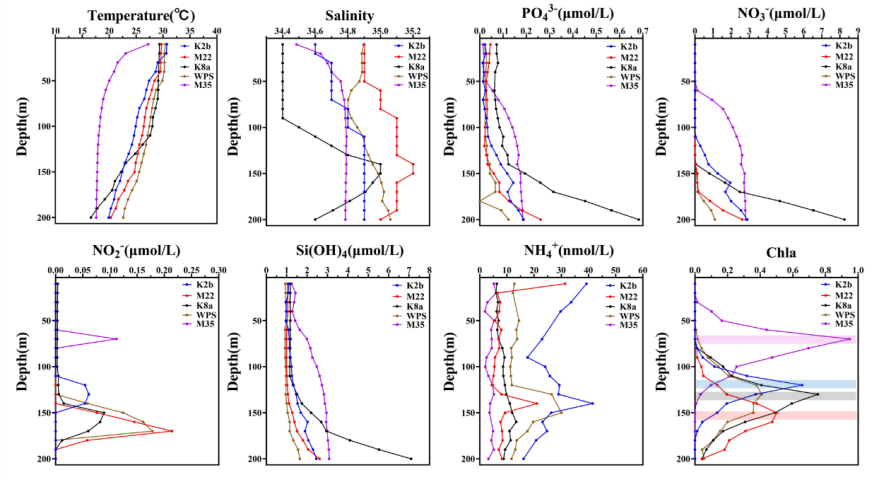

Fig. 2 Vertical profiles of temperature, salinity, nutrients, and chlorophyll *a* within the 0-200 m layer during summer season. In the Chl *a* graph, the strip-shaped color blocks represent the approximate positions of the DCM layer at different stations. The depths of the DCM at stations K8b and WPS almost coincide.

Within this physicochemical framework, diatom communities, diatom abundance, and estimated carbon biomass showed significant spatial and vertical heterogeneity ($P<0.05$) (Fig. 3a-c). Summer averages of abundance and estimated carbon biomass across the regions were 235 ± 526 cells L^{-1} and 114.2 ± 311.3 ng C L^{-1}, with peaks located within the DCM layer of stations influenced by the Kuroshio Extension and Kuroshio (M35, K2b) (Fig. 3b, d). Vertical profiles revealed that maximum diatom carbon biomass generally coincided with the DCM, except at station WPS, where non-diatom groups likely dominated the DCM community (Fig. 3d). Notably, winter biomass in the mixed layer at stations M22 and K8a exceeded summer values, underscoring seasonal dynamics (Fig. 3e).

https://doi.org/10.5194/egusphere-2026-2
Preprint. Discussion started: 21 January 2026

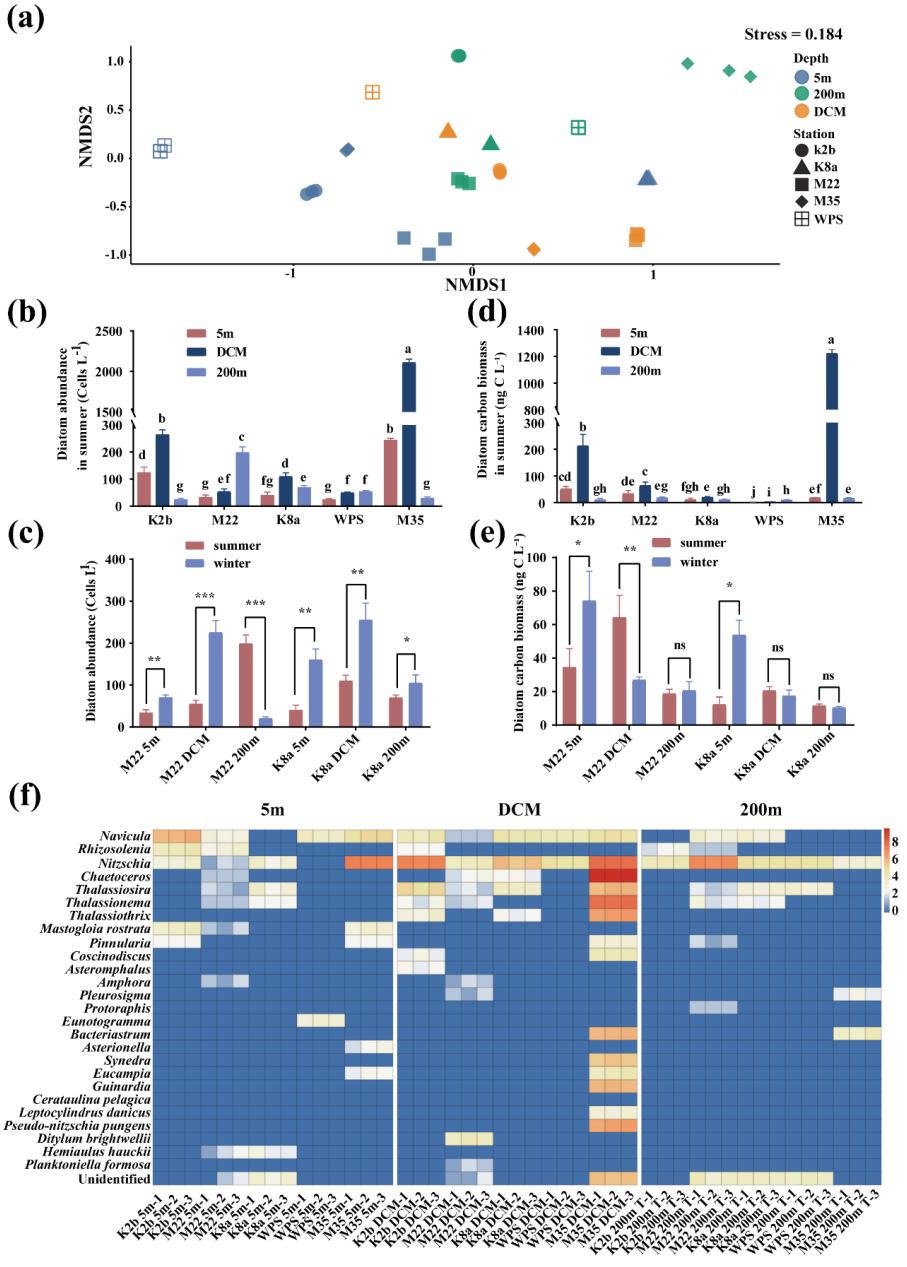

Fig. 3 The regional heterogeneity of diatom communities, abundance, estimated carbon biomass, and dominated species in the western North Pacific Subtropical Gyre (NPSG). (a) Non-metric MultiDimensional Scaling (NMDS) of Bray–Curtis dissimilarity between ribotag profiles for diatom communities. Each colored symbol represents a biological replicate. (b) Abundance of diatoms at three depths across five

https://doi.org/10.5194/egusphere-2026-2
Preprint. Discussion started: 21 January 2026

stations in summer, (c) Estimated carbon biomass of diatoms at three depths across five stations in summer, (d) Comparison of diatom abundance between summer and winter, (e) Comparison of diatom carbon biomass estimates between summer and winter. (f) Heat map depicting the relative abundance of diatoms in the water column. KE: Kuroshio Extension area; NEC: North Equatorial Current. The DCM layer depths in summer for stations K2b, WPS, M22, K8a, and M35 are 110 m, 145 m, 155 m, 150 m, and 95 m, respectively. In winter, the DCM layer depths for stations M22 and K8a are 135 m and 146 m, respectively.

Community composition analysis identified 37 taxa from 26 genera during summer, displaying clear vertical niche differentiation linked to the nutrient gradients. Taxa such as *Navicula* and *Rhizosolenia* exhibited higher abundance in the NDL than in the NRL, whereas *Nitzschia*, *Chaetoceros*, and *Thalassiosira* tended to be dominant in the NRL (Fig. 3f). The contribution of different genera to community carbon biomass varied widely: large-celled *Rhizosolenia* dominated the biomass at the mixed surface (5m) of stations K2b, while the small but ubiquitous *Nitzschia* was the most frequently occurring taxon (Table S3). This structured community distribution sets the stage for understanding differential contributions to export.

3.2. Spatial and temporal variability in diatom diversity

Diatom α-diversity, assessed through species richness, evenness, and the Simpson index (based on estimated carbon biomass), varied significantly across stations and seasons ($P < 0.05$) (Fig. 4, Tables S4, S5). During summer, station M22 within the gyre interior supported significantly higher species richness than stations K8a ($P < 0.01$) and WPS ($P < 0.01$) (Fig. 4a). The Simpson index at WPS was significantly lower than that at K8a ($P < 0.05$) and M35 ($P < 0.05$) (Fig. 4c), indicating weaker diversity at WPS. Seasonal comparisons revealed higher richness at M22 in summer than in winter (Fig. 4d), while carbon biomass was more evenly distributed among species at K8a during winter based on Pielou evenness (Fig. 4e). These patterns highlight that diversity is not static but responds to regional physicochemical settings and seasonal forcing.

https://doi.org/10.5194/egusphere-2026-2
Preprint. Discussion started: 21 January 2026

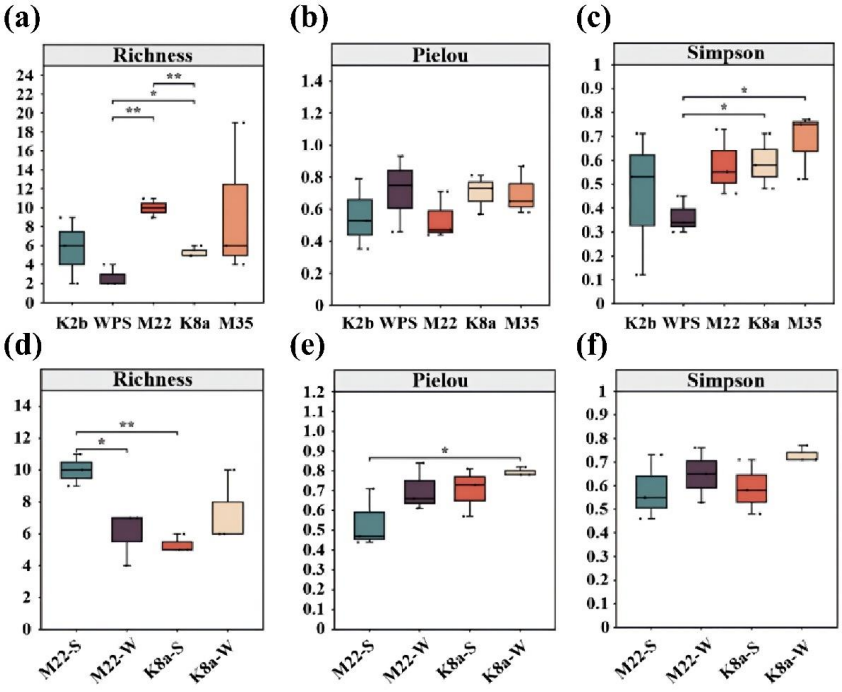

Fig. 4 Alpha diversity index of the diatom community. (a, d) Richness index; (b, e) Pielou evenness index; (c, f) Simpson index. (a-c) Alpha diversity indices during the summer season. (d-f) Comparison of alpha diversity indices between summer and winter. "M22-S," "M22-W," "K8a-S," and "K8a-W" represent M22-summer, M22-winter, K8a-summer, and K8a-winter, respectively. The boxes indicate the ranges of the first and third quartiles, the line inside each box represents the median, and the whiskers show the lowest and highest data points (mean ± 1.5 SD). Note that Simpson's index is presented as 1-D. Asterisks indicate statistically significant results (*$p < 0.05$; **$p < 0.01$).

3.3. Linking diatom communities to environmental drivers

Spearman's correlation analysis revealed key relationships between dominant diatom taxa and environmental factors, underscoring niche specialization (Fig. 5). In summer, *Rhizosolenia* abundance showed a strong positive correlation with ammonium (NH_4^+, $r = 0.72$, $P < 0.01$). Conversely, *Navicula*, a similar dominant species in the mixed layer, exhibited a negative correlation with depth, NO_3^-, and $NO_3^- + NO_2^-$ ($r = -0.53$, $P < 0.05$; $r = -0.53$, $P < 0.05$, respectively). *Nitzschia*, *Chaetoceros*, *Thalassiosira*,

https://doi.org/10.5194/egusphere-2026-2
Preprint. Discussion started: 21 January 2026

364 which are prevalent in the DCM, were positively correlated with Chl *a* (r =0.61, P<
365 0.05; r =0.53, P< 0.05; r = 0.53, P< 0.05; r = 0.55, P < 0.05, respectively) (Fig. 5a).
366 Regardless of whether it is summer or winter, the abundance of the widespread genus
367 *Nitzschia* was correlated with total diatom abundance (r = 0.82, P < 0.01; r = 0.94,
368 P<0.05, respectively), which confirms its central role in the community (Fig. 5). These
369 correlations demonstrate that the vertical stratification of diatom taxa is underpinned by
370 distinct physiochemical affinities.
371

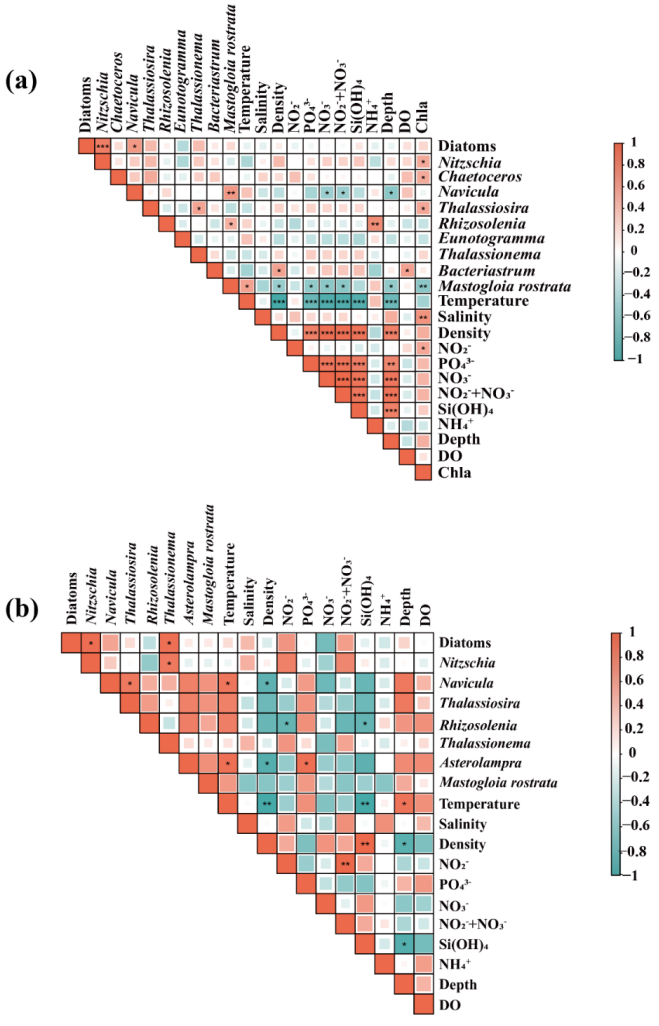

372

373 **Fig. 5 Spearman′s correlation between diatoms and environmental factors.** (a) In
374 summer. (b) In winter. NO_2^-: nitrite, PO_4^{3-}: phosphate, NO_3^-: nitrate, Si $(OH)_4$: silicic

https://doi.org/10.5194/egusphere-2026-2
Preprint. Discussion started: 21 January 2026

acid, NH_4^+: ammonium, DO: dissolved oxygen, Chl *a*: chlorophyll *a*. Asterisks indicate statistically significant results: *p< 0.05, ** p < 0.01, and *** p < 0.001.

3.4. Magnitude and composition of diatom export flux

Diatom export fluxes, quantified via sediment traps at three stations (K2b, M22, K8a) in summer, revealed substantial heterogeneity (P<0.05) (Fig. 6a, b). Intact cell fluxes ranged from 10^3 to 10^5 cells m^{-2} d^{-1} (Table S6), and the estimated carbon fluxes ranged from 0.13 to 194.85 μg C m^{-2} d^{-1}. The highest fluxes were observed at Station K2b, which is influenced by the Kuroshio (Fig. 6a). This observation is supported by the diatom cells flux, the estimated carbon flux, and the BSi flux (Table 1).

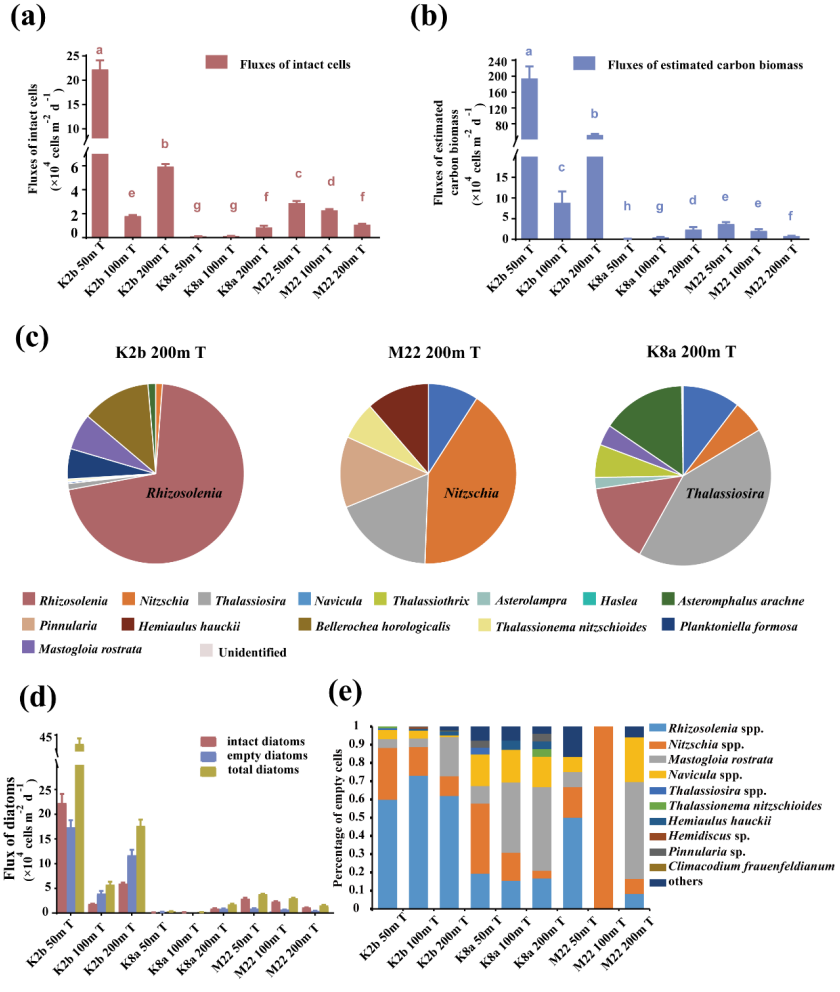

https://doi.org/10.5194/egusphere-2026-2
Preprint. Discussion started: 21 January 2026

Fig. 6 Vertical flux of diatom cells at a depth of 200 m in the western NPSG. (a) Fluxes of intact diatom cells. (b) Fluxes of estimated carbon biomass. Different lowercase letters indicate significant differences in intact cell flux or estimated carbon biomass flux among the samples. (c) Comparison of the relative contributions of diatom genera based on the estimated carbon biomass from the 200 - m depth sediment trap. (d) Total, empty, and intact diatom cells in trap samples. (e) Species composition and relative abundance of empty diatom frustules in trap samples. The labels "K2b 5m", "K2b 150m", and "K2b 200m" denote water samples collected at depths of 5 m, 150 m, and 200 m, respectively, from station K2b. The labels "K2b 50m T", "K2b 100m T", and "K2b 200m T" refer to trap samples collected at corresponding depths of 50 m, 100 m, and 200 m at station K2b. This naming convention is consistently applied to samples from stations M22 and K8a. Twenty liters of water were collected per depth interval for cell abundance analysis, and one sediment trap tube (10 cm diameter × 50 cm height) was used per depth interval for diatom flux analysis.

The taxonomic composition of the exported material directly reflected the vertically stratified source communities. At K2b, export at 200 m was dominated by *Rhizosolenia* (contributing 71% of diatom carbon export), which originated primarily from the mixed layer (Fig. 6c). At stations M22 and K8a, export was dominated by *Nitzschia* and *Thalassiosira*, respectively, both sourced mainly from the DCM layer (Fig. 6c). Notably, a significant fraction of sinking cells were empty frustules (Fig. 6d, e), indicating active bacterial degradation of organic matter during sinking, particularly for *Rhizosolenia* and *Nitzschia*.

3.5. Regional heterogeneity in diatom-mediated export efficiency

A notable regional disparity in the efficiency of diatom production export was identified (Table 1). We defined export efficiency here by comparing the diatom export proportion (DEP) at 200 m to the diatom production proportion (DPP) (Table S7, S8). Station K2b exhibited high efficiency (DEP > DPP), driven by the large, carbon-rich *Rhizosolenia*, which also resulted in a high diatom carbon flux to biogenic silica (BSi) flux ratio, indicating a community of lightly silicified cells. Station K8a showed a similar but less pronounced trend (moderate). In stark contrast, station M22 in the gyre interior showed low efficiency (DEP < DPP) despite having the highest total POC flux,

https://doi.org/10.5194/egusphere-2026-2
Preprint. Discussion started: 21 January 2026

implying a greater relative contribution from non-diatom phytoplankton to export at this site. This demonstrates that diatom carbon export efficiency is decoupled from total POC flux and is instead regulated by regional differences in diatom community structure and functional traits.

Table 1 Comparison of diatom cell flux, estimated carbon flux, BSi flux, and export efficiency at 200m depth across three stations in the western NPSG during summer

Parameters	K2b (Kuroshio)	M22 (NPSG interior)	K8a (NEC)
Diatom cell flux [cells m^{-2} d^{-1}]	6.0 * 10^4	1.1 * 10^4	0.9* 10^4
Diatom estimated carbon flux (µg C m^{-2} d^{-1})	52.4	0.79	2.42
BSi flux [mmol m^{-2} d^{-1}]	0.19	0.06	0.04
Export efficiency	High (DEP>DPP)	low (DEP<DPP)	moderate (DEP>DPP)
Diatom export proportion (DEP)	17.2 %	0.8 %	1.4%
Diatom production proportion (DPP)	1.2-6.8%	1.5-2.0%	0.7-1.1%
Total POC flux [mmol C m^{-2} d^{-1}]	3.19	3.67	0.92
Diatom estimated carbon flux/POC flux	0.14%	0.002%	0.022%
Diatom estimated carbon flux/BSi flux	0.02	0.001	0.005
Diatom species	High DDA	Low DDA	Low DDA

BSi: biogenic silica; POC flux: particulate organic carbon flux; DDA: diatom–diazotroph associations; Diatom production proportion: the ratio of diatom carbon production to the total carbon production of phytoplankton within the water column; Diatom export proportion: the ratio of diatom carbon export flux to the total phytoplankton carbon export flux.

3.6. Metagenomic evidence for limited bacterial degradation of key diatom polymers

https://doi.org/10.5194/egusphere-2026-2
Preprint. Discussion started: 21 January 2026

Metagenomic analysis of water bacteria across five stations assessed the genetic potential for degrading diatom-derived organic matter (Fig. 7). The high relative abundance of glycosyl transferases (GT) and glycoside hydrolases (GH) within the six functional CAZyme modules (Fig. 7a) indicates a bacterial community adapted for both polysaccharide synthesis (GT) and degradation (GH), highlighting its pivotal role in the processing of environmental carbohydrates, including diatom- derived POC.

While genes for degrading common diatom polysaccharides like laminarin (e.g. GH16, GH17, GH30, GH3, Unfried et al., 2019) and mannan (e.g. GH26, GH2, GH92, GH3, GH130, GH88, Kappelmann et al., 2018) were widespread and taxonomically diverse (Fig. 7b, c), a key gene for cleaving the sulfated fucan backbone of FCSPs—glycoside hydrolase 107 (GH107) (Nagao et al., 2017)—was notably scarce or absent (Fig. 7d, e). Given that dominant diatoms in this region (e.g., *Chaetoceros*, *Thalassiosira*, *Nitzschia*) are known FCSP producers (Huang et al., 2021; Vidal-Melgosa et al., 2021), this genetic deficit suggests a limited bacterial capacity to degrade this specific polymer. Furthermore, genomic analysis of key degraders like Bacteroidetes revealed few polysaccharide utilization loci (PULs), and none targeting FCSPs (Fig. S1). This implies that diatom-derived FCSPs may resist rapid microbial breakdown, potentially enhancing the preservation and export of diatom-associated carbon.

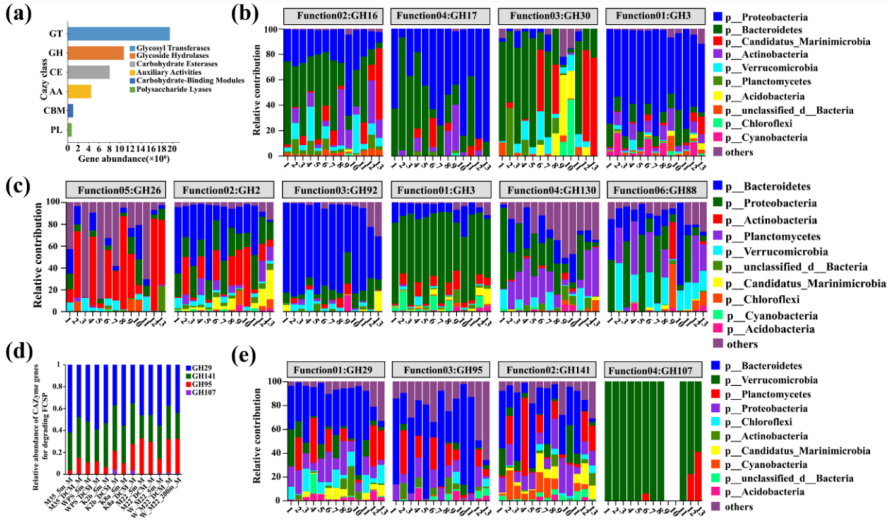

https://doi.org/10.5194/egusphere-2026-2
Preprint. Discussion started: 21 January 2026

Fig. 7 Composition and abundance of CAZyme genes, along with the contribution of dominant microbial groups at the phylum level. (a) CAZyme gene composition and abundance detected in this study. (b) Contribution of dominant microbial groups to CAZymes for degrading laminarin. (c) Contribution of dominant microbial groups to CAZymes for degrading laminarin mannans. (d) Composition and relative abundance of CAZyme genes for degrading fucose-containing sulfated polysaccharides (FCSP). (e) Contribution of dominant microbial groups to CAZymes for degrading FCSP. "M35_ 5m_ M" and "M35_ DCM_M" denote water samples collected at depths of 5 m and the depth of maximum chlorophyll *a* (DCM), respectively, from station M35 during the summer cruise for metagenomic analysis. This naming convention is consistently applied to samples from four additional stations (WPS, K2b, M22, and K8a). "W_M22_ 5m_M", "W_M22_DCM_M", and "W_M22_ 200m_M" refer to water samples collected at depths of 5 m, DCM, and 200 m, respectively, from station M22 during the winter cruise for metagenomic analysis. Samples "1" to "10" represent summer collections at M35_5m, M35_DCM, WPS_5m, WPS_DCM, K2b_5m, K2b_DCM, K8a_5m, K8a_DCM, M22_5m, and M22_DCM, while "11", "12", and "13" represent winter collections at M22_5m, M22_DCM, and M22_200m, respectively. Taxa with a relative abundance below 0.01 in all samples were aggregated into the category "others".

4. Discussion

4.1. Diatom export fluxes: establishing a baseline and contextualizing heterogeneity

This study provides a quantitative baseline for diatom abundance and carbon export in the western NPSG. The observed diatom abundance (mean: 235 ± 526 cells L^{-1}) and cell export fluxes (10^3–10^5 cells m^{-2} d^{-1}) align with the lower range typical of stratified oligotrophic oceans (Table S9, S10) (Lange et al., 1998; Girault et al., 2016; Ding et al., 2021; Wei et al., 2021). This consistency underscores the characteristically low but measurable role of diatoms in these systems. Critically, the pronounced spatial heterogeneity in fluxes—spanning orders of magnitude within the gyre—reveals that oligotrophy does not equate to negligible export. Instead, it masks a mosaic of biogeochemical provinces where specific physical-biological interactions can episodically enhance carbon transfer. In the context of climate-driven expansion of oligotrophic gyres (Cabré et al., 2015), our data highlight that intrinsic heterogeneity

https://doi.org/10.5194/egusphere-2026-2
Preprint. Discussion started: 21 January 2026

will persist, necessitating regionally refined models to project future carbon cycling.

4.2. Physico-chemical drivers of diatom community structure and export potential

The observed coupling between diatom community composition and vertical nutrient gradients emphasizes nutrient supply as a factor controlling export-relevant taxa. In the NPSG, nutrient delivery is modulated by a suite of physical and biogeochemical processes, including eddy activity, nitrogen fixation, and lateral advection (Karl et al., 1997, 2012; Letscher et al., 2016; Xiu & Chai, 2020). Our observations are consistent with such mechanisms: for instance, DCM community at station M35, dominated by *Thalassiosira* and *Chaetoceros*, likely benefited from nutrient injections associated with North Pacific Tropical Subtropical Mode Water (Du et al., 2024). This link implies that future changes in ocean stratification and subsurface nutrient dynamics will not only affect total productivity but also reconfigure the functional structure of export-prone diatom communities, with direct consequences for carbon sequestration.

4.3. Regional heterogeneity in export efficiency: a trait-based and mechanistic perspective

A crucial discovery in our research is the notable regional heterogeneity in the carbon export efficiency of diatoms. The hotspot at station K2b was driven by diatom-diazotroph assemblages (DDAs, e.g., *Rhizosolenia* spp.), which combine high cellular carbon content with an ecological strategy linked to nitrogen fixation. The spatial co-occurrence of elevated ammonium (Fig. 2 and Shen et al., 2024), *Trichodesmium* blooms (Jiang et al., 2025), and high *Rhizosolenia* abundance suggests a tight biogeochemical coupling where fixed nitrogen supports high-carbon-content diatom production (Dai et al., 2023; Shen et al., 2024), thereby enhancing export efficiency.

In contrast, export at station K8a was dominated by *Thalassiosira* spp., demonstrating a different, moderately efficient pathway. The gyre interior (M22) showed the lowest efficiency, despite *Nitzschia* spp. dominating the flux, highlighting that species-specific traits—such as carbon content, nutrient affinity, and aggregate formation potential—are critical determinants of flux efficiency rather than abundance alone. Under climate change, shifts in the competitive landscape for these different ecological strategies will likely alter the functional composition of export fluxes,

https://doi.org/10.5194/egusphere-2026-2
Preprint. Discussion started: 21 January 2026

impacting the strength of the biological pump.

4.4. The biogeochemical role of diatom polymers in carbon flux

Beyond bulk community traits, our metagenomic analysis points to a molecular-scale mechanism influencing carbon export: the fate of diatom-derived FCSPs. These biopolymers are key agents in forming transparent exopolymer particles (TEP), which enhance particle aggregation and exhibit resistance to degradation (Passow et al., 2001; Huang et al., 2021). In the macroalgae-scarce western NPSG, dominant diatom genera (e.g., *Chaetoceros*, *Thalassiosira*, *Nitzschia*) are major FCSP producers, positioning them as potential architects of aggregate formation and carbon export. The limited genetic potential for FCSP degradation in the water bacterial community we observed suggests a potential mechanism for enhanced carbon flux preservation.

In an ecosystem dominated by small phytoplankton, diatom-derived FCSPs may act as crucial biogeochemical "glue", facilitating the coagulation and export of otherwise slow-sinking picoplankton (Albertano et al., 1997; Richardson & Jackson, 2007; Guidi et al., 2016). This potential cross-functional facilitation underscores the interconnectedness of phytoplankton guilds in driving carbon flux. As future oceans become more stratified and dominated by smaller cells (Ali et al., 2025), the role of such conditioning agents in sustaining particle export may become increasingly critical, making the environmental drivers of FCSP production and lability a key research frontier for projecting biological pump resilience.

4.5. Key taxa and functional traits governing long-term sequestration

The contribution of diatoms to POC export is governed by a suite of species-specific functional traits. *Rhizosolenia*, with its large size and high carbon content, acted as a major export vector at K2b, consistent with observations of its role in deep export events elsewhere (~4000 m; Karl et al., 2012). Its potential for rapid, aggregate-mediated sinking (Agusti et al., 2015) is supported by our inference of FCSP production.

Conversely, the smaller *Nitzschia*, which dominated fluxes at other stations, represents a high-efficiency pathway for organic carbon export relative to silica (low Si/C ratio, Brzezinski, 1985), favoring long-term sequestration once carbon is transferred to depth (1,003 m, Sabine et al., 2004; Ran et al., 2015; Zhang et al., 2018). Other taxa like *Thalassiosira* and *Chaetoceros* possess traits (e.g., resting spores,

https://doi.org/10.5194/egusphere-2026-2
Preprint. Discussion started: 21 January 2026

polymer exudation) (Rembauville et al., 2016; Huang et al., 2021; Vidal-Melgosa et al., 2021), that predispose them to enhanced export. These findings collectively demonstrate that predicting the ocean's carbon sink requires a trait-based approach that accounts for the biogeography and success of key functional groups, not just total biomass.

5. Conclusion

This study demonstrates that diatom-mediated carbon export in the oligotrophic western NPSG is characterized by significant vertical structuring and regional heterogeneity, driven by the interplay of physical, chemical, and biological processes. We show that export is not a simple function of total diatom abundance but is fundamentally regulated by: 1) Hydrographic controls that create distinct nutrient regimes and shape diatom community composition. 2) Species-specific functional traits, such as cell size, carbon content, and the production of aggregation-promoting biopolymers (FCSPs), which determine the quality and efficiency of export. 3) Cross-ecosystem interactions, where processes like nitrogen fixation can fuel hotspots of high export efficiency, and diatom-derived polymers may facilitate the export of co-occurring smaller plankton.

Even within an oligotrophic gyre, these interacting mechanisms can sustain regionally efficient carbon export, challenging simplistic paradigms of low biological pump activity. Our integrated analysis provides a mechanistic, process-oriented framework for understanding and projecting the heterogeneity of marine carbon sequestration. Future research must prioritize long-term, multitrophic observations and mechanistic studies to quantify how these critical interactions will respond to global change, thereby refining our predictions of the ocean's evolving carbon sink.

Acknowledgements

This work was supported by the National Natural Science Foundation of China (grant number: 41890804, 42076115). Environmental data were kindly provided by Dr. Xianghui Guo and Zhimian Chao from College of Ocean and Earth Sciences, Xiamen University, Xiamen, China.

Author contributions

https://doi.org/10.5194/egusphere-2026-2
Preprint. Discussion started: 21 January 2026

Feng Li: Investigation, Writing - original draft, Formal analysis; Hongzhen Jiang: Investigation, Visualization; Zhouyi Jiang: Formal analysis, Visualization; Linwei Liu: Formal analysis, Visualization; Lu Huang: Formal analysis, Visualization; Kehui Feng: Formal analysis, Visualization; Zuozhu Wen: Investigation; Xin Liu: Investigation; Changping Chen: Resources; Kuanbo Zhou: Investigation, Formal analysis; Junrong Liang: Conceptualization, Funding acquisition, Resources, Writing - original draft, Validation, Writing - review & editing. The final manuscript was approved by all the authors.

Data availability

Data will be made available on request. The data that supports the findings of this study are available in the supplementary material of this article.

Declaration of competing interest

The authors declare that they have no known competing financial interests or personal relationships that could have appeared to influence the work reported in this paper

https://doi.org/10.5194/egusphere-2026-2
Preprint. Discussion started: 21 January 2026

References

1) Agusti, S., González-Gordillo, J. I., Vaqué, D., Estrada, M., Cerezo, M. I., Salazar, G., Gasol, J. M., and Duarte, C. M.: Ubiquitous healthy diatoms in the deep sea confirm deep carbon injection by the biological pump, Nat Commun., 6, 7608, https://doi.org/10.1038/ncomms8608, 2015.

2) Albertano, P., Somma, D. D., and Capucci, E.: Cyanobacterial picoplankton from the Central Baltic Sea: cell size classification by image-analyzed fluorescence microscopy, J Plankton Res., 19, 1405–1416, https://doi.org/10.1093/plankt/19.10.1405, 1997.

3) Ali, S. M., Kuttippurath, J., Krishna, A. V., Gupta, A., Ganguly, D., P, A., Raman, M., Sahay, A., and Babu, K. N.: An in-depth analysis of the impact of environmental drivers on the variability of phytoplankton community in the Arabian Sea during 2010–2021, Environ. Sci.: Processes Impacts., 27, 498–512, https://doi.org/10.1039/D4EM00385C, 2025.

4) Belcher, A., Henley, S. F., Hendry, K., Wootton, M., Friberg, L., Dallman, U., Wang, T., Coath, C., and Manno, C.: Seasonal cycles of biogeochemical fluxes in the Scotia Sea, Southern Ocean: a stable isotope approach, Biogeosciences, 20, 3573–3591, https://doi.org/10.5194/bg-20-3573-2023, 2023.

5) Brzezinski, M. A.: The Si:C:N ratio of marine diatoms: interspecific variability and the effect of some environmental variables, J. Phycol., 21, 347–357, https://doi.org/10.1111/j.0022-3646.1985.00347.x, 1985.

6) Buzas, M. A. and Hayek, L.-A. C.: On richness and evenness within and between communities, Paleobiology, 31, 199–220, http://www.jstor.org/stable/4096804, 2005.

7) Cao, Z., Wang, D., Zhang, Z., Zhou, K., Liu, X., Wang, L., Huang, B., Cai, P., and Dai, M.: Seasonal dynamics and export of biogenic silica in the upper water column of a large marginal sea, the northern South China Sea, Prog Oceanogr., 188, 102421, https://doi.org/10.1016/j.pocean.2020.102421, 2020.

8) Cabré, A., Marinov, I., and Leung, S.: Consistent global responses of marine ecosystems to future climate change across the IPCC AR5 earth system models, Clim Dyn., 45, 1253–1280, https://doi.org/10.1007/s00382-014-2374-3, 2015.

9) Chen, D., Shi, Z., Li, R., Li, X., Cheng, Y., and Xu, J.: Hydrodynamics drives shifts in phytoplankton community composition and carbon-to-chlorophyll a ratio in the

https://doi.org/10.5194/egusphere-2026-2
Preprint. Discussion started: 21 January 2026

northern South China Sea, Front. Mar. Sci., 10, 1293354, https://doi.org/10.3389/fmars.2023.1293354, 2023.

10) Chitari, R. R. and Anil, A. C.: Estimation of diatom and dinoflagellate cell volumes from surface waters of the Northern Indian Ocean, Oceanologia, 59, 389–395, https://doi.org/10.1016/j.oceano.2017.03.001, 2017.

11) Dai, M., Luo, Y., Achterberg, E. P., Browning, T. J., Cai, Y., Cao, Z., Chai, F., Chen, B., Church, M. J., Ci, D., Du, C., Gao, K., Guo, X., Hu, Z., Kao, S., Laws, E. A., Lee, Z., Lin, H., Liu, Q., Liu, X., Luo, W., Meng, F., Shang, S., Shi, D., Saito, H., Song, L., Wan, X. S., Wang, Y., Wang, W., Wen, Z., Xiu, P., Zhang, J., Zhang, R., and Zhou, K.: Upper Ocean Biogeochemistry of the Oligotrophic North Pacific Subtropical Gyre: From Nutrient Sources to Carbon Export, Rev Geophys., 61, e2022RG000800, https://doi.org/10.1029/2022RG000800, 2023.

12) Ding, C., Sun, J., Narale, D., and Liu, H.: Phytoplankton Community in the Western South China Sea in Winter and Summer, Water, 13, 1209, https://doi.org/10.3390/w13091209, 2021.

13) Dixon, P.: VEGAN, a package of R functions for community ecology, J Vegetation Science., 14, 927–930, https://doi.org/10.1111/j.1654-1103.2003.tb02228.x, 2003.

14) Dore, J. E., Letelier, R. M., Church, M. J., Lukas, R., and Karl, D. M.: Summer phytoplankton blooms in the oligotrophic North Pacific Subtropical Gyre: Historical perspective and recent observations, Prog Oceanogr., 76, 2–38, https://doi.org/10.1016/j.pocean.2007.10.002, 2008.

15) Du, C., Dai, M., Liu, Z., Hu, Z., Yang, J.-Y. T., Zhou, K., Lin, H., Yuan, Z., Wang, L., Huang, T., Guo, L., Wang, Z., and Kao, S.-J.: Diapycnal Fluxes of Nutrients in the North Pacific Subtropical Gyre, Global Planet. Change (to accepted).,https://doi.org/10.2139/ssrn.4915323, 2024.

16) Eppley, R. W., Reid, F., and Strickland, J.: Estimates of phytoplankton crop size, growth rate, and primary production, Calif Univ Scripps Inst Oceanogr Bull., 1970.

17) Fu, L., Niu, B., Zhu, Z., Wu, S., and Li, W.: CD-HIT: accelerated for clustering the next-generation sequencing data, Bioinformatics, 28, 3150–3152, https://doi.org/10.1093/bioinformatics/bts565, 2012.

18) Guidi, L., Chaffron, S., Bittner, L., Eveillard, D., Larhlimi, A., Roux, S., Darzi, Y., Audic, S., Berline, L., Brum, J. R., Coelho, L. P., Espinoza, J. C. I., Malviya, S., Sunagawa, S., Dimier, C., Kandels-Lewis, S., Picheral, M., Poulain, J., Searson, S.,

https://doi.org/10.5194/egusphere-2026-2
Preprint. Discussion started: 21 January 2026

672 Tara Oceans Consortium Coordinators, Stemmann, L., Not, F., Hingamp, P.,
673 Speich, S., Follows, M., Karp-Boss, L., Boss, E., Ogata, H., Pesant, S.,
674 Weissenbach, J., Wincker, P., Acinas, S. G., Bork, P., De Vargas, C., Iudicone, D.,
675 Sullivan, M. B., Raes, J., Karsenti, E., Bowler, C., and Gorsky, G.: Plankton
676 networks driving carbon export in the oligotrophic ocean, Nature, 532, 465–470,
677 https://doi.org/10.1038/nature16942, 2016.
678 19) Girault, M., Gregori, G., Barani, A., and Arakawa, H.: A study of
679 microphytoplankton and cyanobacteria consortia in four oligotrophic regimes in
680 the western part of the North Pacific subtropical gyre and in the warm pool, J.
681 Plankton Res., 38, 1317–1333, https://doi.org/10.1093/plankt/fbw056, 2016.
682 20) Harrison, P. J., Zingone, A., Mickelson, M. J., Lehtinen, S., Ramaiah, N., Kraberg,
683 A. C., Sun, J., McQuatters-Gollop, A., and Jakobsen, H. H.: Cell volumes of marine
684 phytoplankton from globally distributed coastal data sets, Estuar Coast Shelf S.,
685 162, 130–142, https://doi.org/10.1016/j.ecss.2015.05.026, 2015.
686 21) Henson, S., Le Moigne, F., and Giering, S.: Drivers of Carbon Export Efficiency
687 in the Global Ocean, Global Biogeochemical Cy., 33, 891–903,
688 https://doi.org/10.1029/2018GB006158, 2019.
689 22) Huang, B., Hu, J., Xu, H., Cao, Z., and Wang, D.: Phytoplankton community at
690 warm eddies in the northern South China Sea in winter 2003/2004, Deep-Sea
691 Research II., 57, 1792–1798, https://doi.org/10.1016/j.dsr2.2010.04.005, 2010.
692 23) Huang, G., Vidal-Melgosa, S., Sichert, A., Becker, S., Fang, Y., Niggemann, J.,
693 Iversen, M. H., Cao, Y., and Hehemann, J.: Secretion of sulfated fucans by diatoms
694 may contribute to marine aggregate formation, Limnol. Oceanogr., 66, 3768–3782,
695 https://doi.org/10.1002/lno.11917, 2021.
696 24) Jiang, R., Hong, H., Wen, Z., Yu, X., Browning, T. J., Chen, Z., Shang, Y., Liu,
697 X., Cao, Z., Achterberg, E. P., Dai, M., and Shi, D.: Significant contribution of the
698 unicellular cyanobacterium UCYN-B to oceanic nitrogen fixation, Natl. Sci. Rev.,
699 12, nwaf337, https://doi.org/10.1093/nsr/nwaf337, 2025.
700 25) Jiang, Z., Gao, Y., Chen, Y., Du, P., Zhu, X., Liao, Y., Liu, X., and Zeng, J.: Spatial
701 heterogeneity of phytoplankton community shaped by a combination of
702 anthropogenic and natural forcings in a long narrow bay in the East China Sea,
703 Estuar Coast Shelf S., 217, 250–261, https://doi.org/10.1016/j.ecss.2018.11.028,
704 2019.

https://doi.org/10.5194/egusphere-2026-2
Preprint. Discussion started: 21 January 2026

26) Kappelmann, L., Krüger, K., Hehemann, J.-H., Harder, J., Markert, S., Unfried, F., Becher, D., Shapiro, N., Schweder, T., Amann, R. I., and Teeling, H.: Polysaccharide utilization loci of North Sea *Flavobacteriia* as basis for using SusC/D-protein expression for predicting major phytoplankton glycans, ISME J., 13, 76–91, https://doi.org/10.1038/s41396-018-0242-6, 2019.

27) Karl, D. M., Church, M. J., Dore, J. E., Letelier, R. M., and Mahaffey, C.: Predictable and efficient carbon sequestration in the North Pacific Ocean supported by symbiotic nitrogen fixation, Proc. Natl. Acad. Sci. U.S.A., 109, 1842–1849, https://doi.org/10.1073/pnas.1120312109, 2012.

28) Karl, D., Letelier, R., Tupas, L., Dore, J., Christian, J., and Hebel, D.: The role of nitrogen fixation in biogeochemical cycling in the subtropical North Pacific Ocean, Nature, 388, 533–538, https://doi.org/10.1038/41474, 1997.

29) Kieser, S., Brown, J., Zdobnov, E. M., Trajkovski, M., and McCue, L. A.: ATLAS: a Snakemake workflow for assembly, annotation, and genomic binning of metagenome sequence data, BMC Bioinf., 21, 257, https://doi.org/10.1186/s12859-020-03585-4, 2020.

30) Kunakh, O. M., Volkova, A. M., Tutova, G. F., and Zhukov, O. V.: Diversity of diversity indices: Which diversity measure is better, Biosys. divers., 31, 131–146, https://doi.org/10.15421/012314, 2023.

31) Kwon, E. Y., Primeau, F., and Sarmiento, J. L.: The impact of remineralization depth on the air–sea carbon balance, Nature Geosci., 2, 630–635, https://doi.org/10.1038/ngeo612, 2009.

32) Lam, P. J., Lee, J.-M., Heller, M. I., Mehic, S., Xiang, Y., and Bates, N. R.: Size-fractionated distributions of suspended particle concentration and major phase composition from the U.S. GEOTRACES Eastern Pacific Zonal Transect (GP16), Mar. Chem., 201, 90–107, https://doi.org/10.1016/j.marchem.2017.08.013, 2018.

33) Lange, C. B., Romero, O. E., Wefer, G., and Gabric, A. J.: Offshore influence of coastal upwelling off Mauritania, NW Africa, as recorded by diatoms in sediment traps at 2195 m water depth, Deep-Sea Res Pt I., 45, 985–1013, https://doi.org/10.1016/S0967-0637(97)00103-9, 1998.

34) Letscher, R. T., Primeau, F., and Moore, J. K.: Nutrient budgets in the subtropical ocean gyres dominated by lateral transport, Nature Geosci., 9, 815–819, https://doi.org/10.1038/ngeo2812, 2016.

https://doi.org/10.5194/egusphere-2026-2
Preprint. Discussion started: 21 January 2026

35) Li, D., Wang, H., Li, Y., Cao, Y., Wu, K., and Wang, Q.: Current trends and hotspots of etiology of auditory neuropathy in the past 30 years: A bibliometric analysis, J Otol., 19, 113–119, https://doi.org/10.1016/j.joto.2024.07.003, 2024.

36) Liu, X., Xiao, W., Landry, M. R., Chiang, K.-P., Wang, L., and Huang, B.: Responses of Phytoplankton Communities to Environmental Variability in the East China Sea, Ecosystems, 19, 832–849, https://doi.org/10.1007/s10021-016-9970-5, 2016.

37) Menden-Deuer, S. and Lessard, E. J.: Carbon to volume relationships for dinoflagellates, diatoms, and other protist plankton, Limnol. Oceanogr., 45, 569–579, https://doi.org/10.4319/lo.2000.45.3.0569, 2000.

38) McDonnell, A. M. P., Boyd, P. W., and Buesseler, K. O.: Effects of sinking velocities and microbial respiration rates on the attenuation of particulate carbon fluxes through the mesopelagic zone, GBC., 29, 175–193, https://doi.org/10.1002/2014GB004935, 2015.

39) Nagao, T., Kumabe, A., Komatsu, F., Yagi, H., Suzuki, H., and Ohshiro, T.: Gene identification and characterization of fucoidan deacetylase for potential application to fucoidan degradation and diversification, J Biosci Bioeng., 124, 277–282, https://doi.org/10.1016/j.jbiosc.2017.04.002, 2017.

40) Noguchi, H., Park, J., and Takagi, T.: MetaGene: prokaryotic gene finding from environmental genome shotgun sequences, Nucleic Acids Res., 34, 5623–5630, https://doi.org/10.1093/nar/gkl723, 2006.

41) Oksanen, J., Guillaume Blanchet, F., Friendly, M., Kindt, R., Legendre, P. McGlinn, D., Minchin, P. R., O'Hara, R. B., Simpson, G. L., Solymos, P., Stevens, M. H. H., Szoecs, E., Wagner, H.: vegan: Community Ecology Package. R package version 2.5-6. URL https://CRAN.R-project.org/package=vegan, 2019.

42) Passow, U., Shipe, R. F., Murray, A., Pak, D. K., Brzezinski, M. A., and Alldredge, A. L.: The origin of transparent exopolymer particles (TEP) and their role in the sedimentation of particulate matter, Cont Shelf Res., 21, 327–346, https://doi.org/10.1016/S0278-4343(00)00101-1, 2001.

43) Paul, S. S., Mallik, B., Mandal, M., Biswas, B., Sekh, S., and Sarkar, N. S.: Epilithic diatoms as biological water quality indicators--A study in three geographically isolated hill streams in India, J Environ Biol., 37, 275–283, 2016.

https://doi.org/10.5194/egusphere-2026-2
Preprint. Discussion started: 21 January 2026

44) Pielou, E. C.: The measurement of diversity in different types of biological collections, J Theor Biol., 13, 131–144, https://doi.org/10.1016/0022-5193(66)90013-0, 1966.

45) Ran, L., Chen, J., Wiesner, M. G., Ling, Z., Lahajnar, N., Yang, Z., Li, H., Hao, Q., and Wang, K.: Variability in the abundance and species composition of diatoms in sinking particles in the northern South China Sea: Results from time-series moored sediment traps, Deep-Sea Res Pt II., 122, 15–24, https://doi.org/10.1016/j.dsr2.2015.07.004, 2015.

46) Rath, A. R. and Mitbavkar, S.: Diatom community dynamics in a tropical brackish coastal ecosystem from an ecological and biogeochemical perspective: A size-fractionated approach, Cont. Shelf Res., 263, 105039, https://doi.org/10.1016/j.csr.2023.105039, 2023.

47) Rembauville, M., Manno, C., Tarling, G.A., Blain, S., and Salter, I.: Strong contribution of diatom resting spores to deep-sea carbon transfer in naturally iron-fertilized waters downstream of South Georgia, Deep-Sea Res. I, 115, 22–35, http://dx.doi.org/10.1016/j.dsr.2016.05.002, 2016.

48) Richardson, T. L. and Jackson, G. A.: Small Phytoplankton and Carbon Export from the Surface Ocean, Science, 315, 838–840, https://doi.org/10.1126/science.1133471, 2007.

49) Sabine, C. L., Feely, R. A., Gruber, N., Key, R. M., Lee, K., Bullister, J. L., Wanninkhof, R., Wong, C. S., Wallace, D. W. R., Tilbrook, B., Millero, F. J., Peng, T.-H., Kozyr, A., Ono, T., and Rios, A. F.: The Oceanic Sink for Anthropogenic CO_2, Science, 305, 367–371, https://doi.org/10.1126/science.1097403, 2004.

50) Scharek, R., Tupas, L., and Karl, D.: Diatom fluxes to the deep sea in the oligotrophic North Pacific gyre at Station ALOHA, Mar. Ecol. Prog. Ser., 182, 55–67, https://doi.org/10.3354/meps182055, 1999.

51) Schreiber, F., Littmann, S., Lavik, G., Escrig, S., Meibom, A., Kuypers, M.M.M., and Ackermann, M.: Phenotypic heterogeneity driven by nutrient limitation promotes growth in fluctuating environments. Nat. Microbiol. 1: 16055, https://doi.org/10.1038/nmicrobiol.2016.55, 2016.

52) Shen, H., Wan, X. S., Zou, W., Dai, M., Xu, M. N., and Kao, S.-J.: Light-driven integration of diazotroph-derived nitrogen in euphotic nitrogen cycle, Nat Commun., 15, 9193, https://doi.org/10.1038/s41467-024-53067-x, 2024.

https://doi.org/10.5194/egusphere-2026-2
Preprint. Discussion started: 21 January 2026

803 53) Simon, E., Lacour, L., Claustre, H., Bock, N., Cornec, M., Sauzède, R., Schmechtig,
804 C., and Coppola, L.: Linking Surface Phytoplankton Dynamics to Small-Particle
805 Fluxes in the Mesopelagic Zone: Insights From High Latitude Bioregions Using
806 BGC-Argo Floats, GBC., 39, e2024GB008447,
807 https://doi.org/10.1029/2024GB008447, 2025.
808 54) Siqueiros Beltrones, D. A., Echevarría Herrera, E., López-Fuerte, F. O., and
809 Martínez, Y. J.: Species Diversity of Benthic Marine Diatoms from a Natural
810 Protected Area in Cuba, Diversity, 17, 181, https://doi.org/10.3390/d17030181,
811 2025.
812 55) Student: The Probable Error of a Mean, Biometrika, 6, 1,
813 https://doi.org/10.2307/2331554, 1908.
814 56) Stukel, M. R., Irving, J. P., Kelly, T. B., Ohman, M. D., Fender, C. K., and Yingling,
815 N.: Carbon sequestration by multiple biological pump pathways in a coastal
816 upwelling biome, Nat Commun., 14, 2024, https://doi.org/10.1038/s41467-023-
817 37771-8, 2023.
818 57) Sun, J.: Geometric models for calculating cell biovolume and surface area for
819 phytoplankton, J. Plankton Res., 25, 1331–1346,
820 https://doi.org/10.1093/plankt/fbg096, 2003.
821 58) Taurozzi, D. and Scalici, M.: Climbing the elevational gradient: Diatom diversity
822 patterns across temporary ponds, Environ. Res., 285, 122630,
823 https://doi.org/10.1016/j.envres.2025.122630, 2025.
824 59) Tréguer, P., Bowler, C., Moriceau, B., Dutkiewicz, S., Gehlen, M., Aumont, O.,
825 Bittner, L., Dugdale, R., Finkel, Z., Iudicone, D., Jahn, O., Guidi, L., Lasbleiz, M.,
826 Leblanc, K., Levy, M., and Pondaven, P.: Influence of diatom diversity on the
827 ocean biological carbon pump, Nature Geosci., 11, 27–37,
828 https://doi.org/10.1038/s41561-017-0028-x, 2018.
829 60) Unfried, F., Becker, S., Robb, C. S., Hehemann, J.-H., Markert, S., Heiden, S. E.,
830 Hinzke, T., Becher, D., Reintjes, G., Krüger, K., Avcı, B., Kappelmann, L., Hahnke,
831 R. L., Fischer, T., Harder, J., Teeling, H., Fuchs, B., Barbeyron, T., Amann, R. I.,
832 and Schweder, T.: Adaptive mechanisms that provide competitive advantages to
833 marine bacteroidetes during microalgal blooms, ISME J., 12, 2894–2906,
834 https://doi.org/10.1038/s41396-018-0243-5, 2018.

https://doi.org/10.5194/egusphere-2026-2
Preprint. Discussion started: 21 January 2026

61) Utermöhl, H.: Zur Vervollkommnung der quantitativen Phytoplankton-Methodik: Mit 1 Tabelle und 15 abbildungen im Text und auf 1 Tafel, SIL Communications., 1953-1996, 9, 1–38, https://doi.org/10.1080/05384680.1958.11904091, 1958.

62) Vidal-Melgosa, S., Sichert, A., Francis, T. B., Bartosik, D., Niggemann, J., Wichels, A., Willats, W. G. T., Fuchs, B. M., Teeling, H., Becher, D., Schweder, T., Amann, R., and Hehemann, J.-H.: Diatom fucan polysaccharide precipitates carbon during algal blooms, Nat Commun., 12, 1150, https://doi.org/10.1038/s41467-021-21009-6, 2021.

63) Villareal, T. A., Adornato, L., Wilson, C., and Schoenbaechler, C. A.: Summer blooms of diatom-diazotroph assemblages and surface chlorophyll in the North Pacific gyre: A disconnect, J. Geophys. Res., 116, C03001, https://doi.org/10.1029/2010JC006268, 2011.

64) Wang, C., Zhang, K., Cao, Z., Zhou, K., Yuan, Z., Chen, J., Ma, Y., Zhou, B., Liu, X., Cai, Y., Shi, D., and Dai, M.: Size-fractionated C:N:P:Si stoichiometry of particulate matter in the subtropical Western North Pacific, Global Planet. Change., 246, 104732, https://doi.org/10.1016/j.gloplacha.2025.104732, 2025.

65) Wang, L., Huang, B., Liu, X., and Xiao, W.: The modification and optimizing of the CHEMTAX running in the South China Sea, Acta Oceanol. Sin., 34, 124–131, https://doi.org/10.1007/s13131-015-0621-z, 2015.

66) Wei, Y., Wang, X., Gui, J., and Sun, J.: Significant Pico- and Nanoplankton Contributions to Biogenic Silica Standing Stocks and Production Rates in the Oligotrophic Eastern Indian Ocean, Ecosystems, 24, 1654–1669, https://doi.org/10.1007/s10021-021-00608-w, 2021.

67) Xiu, P. and Chai, F.: Eddies Affect Subsurface Phytoplankton and Oxygen Distributions in the North Pacific Subtropical Gyre, Geophys. Res. Lett., 47, e2020GL087037, https://doi.org/10.1029/2020GL087037, 2020.

68) Zhang, A., Liu, H., Li, C., Chen, C., Liang, J., Sun, L., and Gao, Y.: Relationship between toxic and harmful microalgae and environmental factors in typical mariculture areas of East China Sea, J. Ocean. Limnol., 40, 2401–2415, https://doi.org/10.1007/s00343-022-2125-y, 2022.

69) Zhang, C., Dang, H., Azam, F., Benner, R., Legendre, L., Passow, U., Polimene, L., Robinson, C., Suttle, C. A., and Jiao, N.: Evolving paradigms in biological

https://doi.org/10.5194/egusphere-2026-2
Preprint. Discussion started: 21 January 2026

carbon cycling in the ocean, Natl. Sci. Rev., 5, 481–499, https://doi.org/10.1093/nsr/nwy074, 2018.